

Article

A Sewer Dynamic Model for Simulating Reaction Rates of Different Compounds in Urban Sewer Pipe

Tzu-Yi Pai ^{1,*}, Huang-Mu Lo ², Terng-Jou Wan ³, Ya-Hsuan Wang ¹, Yun-Hsin Cheng ¹, Meng-Hung Tsai ¹, Hsuan Tang ¹, Yu-Xiang Sun ¹, Wei-Cheng Chen ¹ and Yi-Ping Lin ¹

¹ Master Program of Environmental Education and Management, Department of Science Education and Application, National Taichung University of Education, Taichung 40306, Taiwan; a110103026@gmail.com (Y.-H.W.); acacia831128@gmail.com (Y.-H.C.); ki2715969@gmail.com (M.-H.T.); shan.908t@gmail.com (H.T.); a0926055876@gmail.com (Y.-X.S.); wade85915@gmail.com (W.-C.C.); amy32343234@gmail.com (Y.-P.L.)

² Department of Environmental Engineering and Management, Chaoyang University of Technology, Wufeng, Taichung 41349, Taiwan; hmlo@cyut.edu.tw

³ Department of Environmental and Safety Engineering, National Yunlin University of Science and Technology, Douliou, Yunlin 64002, Taiwan; wantj@gmail.yuntech.edu.tw

* Correspondence: bai@ms6.hinet.net

Abstract: A sewer dynamic model (SDM), an innovative use of combined models, was established to describe the reactions of compounds in a pilot sewer pipe. The set of ordinary differential equations in the SDM was solved simultaneously using the fourth-order Runge–Kutta algorithm. The SDM was validated by calculating the consistency between the simulation and observation values. After the SDM was validated, the reaction rate was analyzed. For heterotrophs in the water phase and biofilm, their growth rates were greater than the organism decay rate. For ammonia, the supply rate was greater than the consumption rate at the initial time, but the supply rate was smaller than the consumption rate from the 3rd hour. The supply rate was smaller than the consumption rate for the other six compounds. The supply rate of oxygen was smaller than the consumption rate before the 4th hour because of the microorganism activities, and, subsequently, the supply rate was greater than the consumption rate after the 4th hour because of reaeration. The results of this study provide an insight into the reaction rates of different compounds in urban sewer pipes and an urban water network modeling reference for policymaking and regulation.

Keywords: urban sewer pipe; sewer dynamic model; heterotrophic biofilm; reaction rate; consumption rate



Citation: Pai, T.-Y.; Lo, H.-M.; Wan, T.-J.; Wang, Y.-H.; Cheng, Y.-H.; Tsai, M.-H.; Tang, H.; Sun, Y.-X.; Chen, W.-C.; Lin, Y.-P. A Sewer Dynamic Model for Simulating Reaction Rates of Different Compounds in Urban Sewer Pipe. *Water* **2021**, *13*, 1580. <https://doi.org/10.3390/w13111580>

Academic Editors:
Mariacrocetta Sambito and
Gabriele Freni

Received: 7 May 2021

Accepted: 1 June 2021

Published: 3 June 2021

Publisher's Note: MDPI stays neutral with regard to jurisdictional claims in published maps and institutional affiliations.



Copyright: © 2021 by the authors. Licensee MDPI, Basel, Switzerland. This article is an open access article distributed under the terms and conditions of the Creative Commons Attribution (CC BY) license (<https://creativecommons.org/licenses/by/4.0/>).

1. Introduction and Background

Massive amounts of people live in cities. People in urban areas utilize energy, environmental resources and develop the land to suit their living conditions. This affects the type of land utilization, hydrology, and landscape. Meanwhile, pollutants are discharged into the environment, and, consequently, environmental resource patterns will be changed. For various uses in household, commercial, and industrial sectors of city life, water resources are indispensable. However, uninterrupted household, commercial, and industrial sewage effluents result in serious pollution of urban water environments [1]. Therefore, for the purpose of water resource protection in a city, it is essential to establish an urban sewer pipe (USP) network that can convey urban sewage from households, commercial districts, or industries to sewage treatment plants (STPs) [2,3]. Urban sewage always contains complex compounds, especially organic compounds. The major categories of organic compounds are lipids (including fats and oils), carbohydrates, and proteins, respectively. After undergoing hydrolysis and microorganisms' reactions, these large molecular compounds are transformed into smaller ones including carbon, nitrogen, phosphorus, and even sulfide with different oxidized states [4–14]. Problems of odor and micropollutants in sewage

have also caused wide public concern in recent years [15]. Due to the large amount of urban sewage with a high concentration of complicated compounds that flows into the USP network, studying the physical, chemical, and biological reactions in the USP network is necessary.

During conveyance, the sewage quality in the USP network undergoes major changes due to microorganisms' reactions [16]. The water level in the USP is usually shallow, and biofilm always grows on the bottom of the USP. The particulate and soluble compounds undergo reactions in the biofilm and water phase, respectively. The urban sewage quality undergoes either aerobic or anaerobic conditions, which depend on the dissolved oxygen (DO) levels. These microorganisms' reactions in urban sewage and in biomass have been investigated and quantified in previous studies [4–14]. Researchers have established several numerical models in which the kinetics of the Activated Sludge Model (ASM) [5], General Dynamic Model (GDM) [17], and other models [11–14] were adopted to describe the reactions in urban sewage.

Hvitved-Jacobsen et al. [12] proposed a conceptual model of the microbial system in the USP network in terms of wastewater organic matter transformations. The conceptual model of the microbial system was established basically according to ASM [5].

Jiang et al. [2] developed a comprehensive biofilm model to predict pollutant transformation and biofilm growth in sewer biofilms. The results showed that multiple types of biomass evolution and competition occurred in heterogenic biofilms in sewers, including organic oxidation, denitrification, nitrification, sulfate reduction, and sulfide oxidation.

Previous studies have explored microorganisms' reactions with different compounds in the USP network, but reaction rates (RRs) of compounds in the USP network have received little attention. The RRs of compounds in the USP network are still unclear, but a better understanding of the RRs of compounds may lead to good maintenance of the USP network and STP operation. Therefore, the RRs of compounds in the USP network are a profitable and necessary topic. In this context, it is better to clearly identify the RR of compounds in the USP network, and the modeling method is a good tool to accomplish this goal.

2. Objectives

Since the compounds' RRs have been seldom mentioned in previous studies, the objectives of this study are described as follows: (1) To propose a sewer dynamic model (SDM) mainly according to the kinetics of GDM and other models for calculating the RRs of compounds in the water phase and biofilm of USP. Since the kinetics of GDM have only been used in the simulation of activated sludge process for a long time, this paper represents the first report of the innovative use of combined models for the simulation of reaction rates of different compounds in the USP network. (2) To validate the established model by determining the consistency between the simulation values (SV) and observation values (OV) for all types of compounds. The established SDM can be validated when a high consistency is reported. (3) To anatomize the RRs of different compounds in the USP using the established SDM.

3. Methodology

3.1. Pilot Sewer Pipe

A plastic pilot sewer pipe (PSP) 21 m long and 0.15 m in diameter was used for the experiments, as shown in Figure 1. The synthetic sewage flowrate and sewer pipe slope could be controlled. The synthetic sewage temperature in the PSP was controlled at 28 centigrade. The synthetic sewage in the tail tank could be conveyed to the head tank using a pump between these two water tanks. The DO concentration in the recirculation tank was monitored using a DO meter. All units including the pipe, highly concentrated synthesis sewage (HCSS) tank, head tank, recirculate tank, and tail tank were sealed to ensure the recirculated sewage was not being oxygenated.

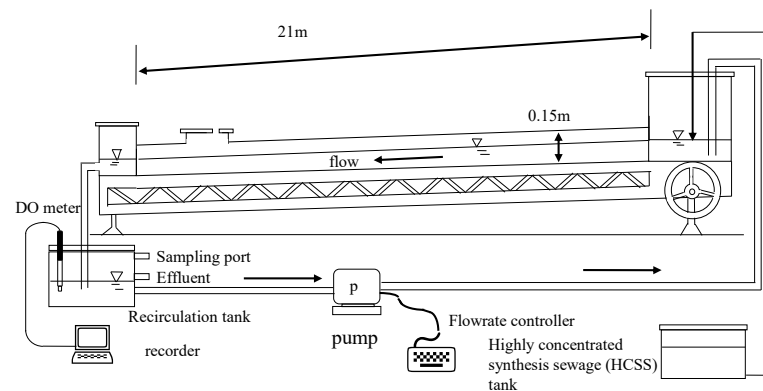


Figure 1. Pilot sewer pipe.

3.2. Experiment Procedures

The HCSS was synthesized using milk powder, sucrose, acetates, and other reagents. For neutralization, a NaOH solution was adopted to control the pH of HCSS at 7–7.5. Table 1 shows the major HCSS compositions. The HCSS was periodically added into the PSP at certain quantities to be mixed with the synthetic sewage in the PSP.

A certain amount of activated sludge was added into the PSP at a fixed influent flowrate. This demonstrated that the biofilm remained in a stable condition if the effluent concentration from the PSP revealed a constant value, i.e., the biofilm grew stably on the PSP bottom. When the batch experiment was finished, the biofilm was acclimated under a steady condition again. The steady flow velocity and the pH were controlled at 0.6 m s^{-1} and 6.0–7.2, respectively. In the experiment, synthetic sewage of 500 mL was taken from the sampling port every 1 h and the concentrations of total chemical oxygen demand (COD), ammonia, nitrate, and DO were analyzed.

Table 1. The compositions of highly concentrated synthetic sewage (HCSS).

Constituents *	Dosage (mg)
Full-fat dry milk powder	163.2
NH ₄ Cl	40.0
Acetates	37.6
Urea	30.0
Sucrose	16.2
KH ₂ PO ₄	15.0
FeCl ₃	0.1
NaOH	For neutralizing

* The constituents were dissolved in 1 L distilled water for synthesizing HCSS.

3.3. Establishment of SDM

When establishing the SDM, several kinetic reaction rate equations (RREs) from previous models were incorporated into GDM [5–7,11–14,18–21]. The GDM kinetics were only used in the simulation of the activated sludge process. In this study, the hydraulic condition was gravity flow in an open channel, neither completely mixing flow nor plug flow in the reactor. The active heterotrophic and autotrophic biomass was separated into two phases, i.e., the water phase and biofilm phase, in the open channel. Furthermore, the reaeration of oxygen in gravity flow was considered. Therefore, this study represents the first report of this innovative use of combined models to simulate the RRs of different compounds in the USP network. The stoichiometric constants and kinetic constants from previous models were also adopted [5–7,11–14,18–21]. Table 2 shows the definitions of compounds in the established SDM. The RREs are shown in Table 3.

Table 2. The definitions of compounds.

Compounds and Definition		Unit
Z _{HW}	Active heterotrophic biomass in the water phase	g COD m ⁻³
Z _{HF}	Active heterotrophic biomass in the biofilm	g COD m ⁻³
Z _{AW}	Active autotrophic biomass in the water phase	g COD m ⁻³
Z _{AF}	Active autotrophic biomass in the biofilm	g COD m ⁻³
Z _E	Endogenous mass	g COD m ⁻³
S _{ENM}	Enmeshed slowly biodegradable substrates	g COD m ⁻³
S _{BCS}	Readily biodegradable “complex” substrate	g COD m ⁻³
N _{BP}	Particulate biodegradable organic nitrogen	g OrgN m ⁻³
N _{BS}	Soluble biodegradable organic nitrogen	g OrgN m ⁻³
N _{H3}	Ammonia-nitrogen	g NH ₃ m ⁻³
N _{O3}	Nitrate and nitrite nitrogen	g NO ₂ ⁻ + NO ₃ ⁻ m ⁻³
S _{O2}	Oxygen	g O ₂ m ⁻³

Table 3. Symbols and definitions for reaction rate equations.

No.	Reaction	Equations
r ₁	Aerobic growth of Z _{HW} in the water phase	$\mu_{ZH}S_{BCS}/(K_{S,ZH} + S_{BCS})S_{O2}/(K_{O,ZH} + S_{O2})Z_{HW}\theta_W^{(T-20)}$
r ₂	Aerobic growth of Z _{HF} in the biofilm	$\mu_{ZH}S_{BCS}/(K_{S,ZH} + S_{BCS})S_{O2}/(K_{O,ZH} + S_{O2})\epsilon Z_{HF}\theta_F^{(T-20)}$
r ₃	Anoxic growth of Z _{HW} in the water phase	$\eta_{GRO}\mu_{ZH}S_{BCS}/(K_{S,ZH} + S_{BCS})K_{O,ZH}/(K_{O,ZH} + S_{O2})N_{O3}/(K_{NO3} + N_{O3})Z_{HW}\theta_W^{(T-20)}$
r ₄	Anoxic growth of Z _{HF} in the biofilm	$\eta_{GRO}\mu_{ZH}S_{BCS}/(K_{S,ZH} + S_{BCS})K_{O,ZH}/(K_{O,ZH} + S_{O2})N_{O3}/(K_{NO3} + N_{O3})\epsilon Z_{HF}\theta_F^{(T-20)}$
r ₅	Aerobic growth of Z _{AW} in the water phase	$\mu_{ZA}N_{H3}/(K_{NH3} + N_{H3})S_{O2}/(K_{O,ZA} + S_{O2})Z_{AW}\theta_W^{(T-20)}$
r ₆	Aerobic growth of Z _{AF} in the biofilm	$\mu_{ZA}N_{H3}/(K_{NH3} + N_{H3})S_{O2}/(K_{O,ZA} + S_{O2})\epsilon Z_{AF}\theta_F^{(T-20)}$
r ₇	Organism decay of Z _{HW} in the water phase	$b_{ZH}Z_{HW}\theta_W^{(T-20)}$
r ₈	Organism decay of Z _{HF} in the biofilm	$b_{ZH}Z_{HF}\theta_F^{(T-20)}$
r ₉	Organism decay of Z _{AW} in the water phase	$b_{ZA}Z_{AW}\theta_W^{(T-20)}$
r ₁₀	Organism decay of Z _{AF} in the biofilm	$b_{ZA}Z_{AF}\theta_F^{(T-20)}$
r ₁₁	Ammonification of N _{BS}	$K_R N_{BS}(Z_{HW}\theta_W^{(T-20)} + Z_{HF}\theta_F^{(T-20)})$
r ₁₂	Hydrolysis of S _{ENM}	$K_H S_{ENM}/(Z_{HW}\theta_W^{(T-20)} + Z_{HF}\theta_F^{(T-20)})/(K_X + S_{ENM}/(Z_{HW}\theta_W^{(T-20)} + Z_{HF}\theta_F^{(T-20)}))(S_{O2}/(K_{O,ZH} + S_{O2})\ddagger + \eta_h K_{O,ZH}/(K_{O,ZH} + S_{O2})N_{O3}/(K_{NO3} + N_{O3}))(Z_{HW}\theta_W^{(T-20)} + Z_{HF}\theta_F^{(T-20)})$
r ₁₃	Hydrolysis of N _{BP}	$K_H N_{BP}/(Z_{HW}\theta_W^{(T-20)} + Z_{HF}\theta_F^{(T-20)})/(K_X + S_{ENM}/(Z_{HW}\theta_W^{(T-20)} + Z_{HF}\theta_F^{(T-20)}))(S_{O2}/(K_{O,ZH} + S_{O2})\ddagger + \eta_h K_{O,ZH}/(K_{O,ZH} + S_{O2})N_{O3}/(K_{NO3} + N_{O3}))(Z_{HW}\theta_W^{(T-20)} + Z_{HF}\theta_F^{(T-20)})$
r ₁₄	Reaeration of oxygen	$K_{La}(S_{O2,SAT} - S_{O2})$ where $K_{La} = 0.96(1 + 0.2F_R^2)(SLOP \cdot V_M)^{3/8}D_H^{-1}\theta_R^{(T-20)}$

By combining the related constants and RREs in Table 3, the complete SDM for all types of compounds can be listed as follows:

$$\frac{dZ_{HW}}{dt} = r_1 + r_3 - r_7 \quad (1)$$

$$\frac{dZ_{HF}}{dt} = r_2 + r_4 - r_8 \quad (2)$$

$$\frac{dZ_{AW}}{dt} = r_5 - r_9 \quad (3)$$

$$\frac{dZ_{AF}}{dt} = r_6 - r_{10} \quad (4)$$

$$\frac{dZ_E}{dt} = f_{ZE} \cdot r_7 + f_{ZE} \cdot r_8 + f_{ZE} \cdot r_9 + f_{ZE} \cdot r_{10} \quad (5)$$

$$\frac{dS_{ENM}}{dt} = (1 - f_{ZE}) \cdot r_7 + (1 - f_{ZE}) \cdot r_8 + (1 - f_{ZE}) \cdot r_9 + (1 - f_{ZE}) \cdot r_{10} - r_{12} \quad (6)$$

$$\frac{dS_{BCS}}{dt} = -\frac{1}{Y_{ZH}} \cdot r_1 - \frac{1}{Y_{ZH}} \cdot r_2 - \frac{1}{Y_{ZH}} \cdot r_3 - \frac{1}{Y_{ZH}} \cdot r_4 + r_{12} \quad (7)$$

$$\frac{dN_{H3}}{dt} = -f_{ZN} \cdot r_1 - f_{ZN} \cdot r_2 - f_{ZN} \cdot r_3 - f_{ZN} \cdot r_4 - (f_{ZN} + \frac{1}{Y_{ZA}}) \cdot r_5 - (f_{ZN} + \frac{1}{Y_{ZA}}) \cdot r_6 + r_{11} \quad (8)$$

$$\frac{dN_{O3}}{dt} = -\frac{1 - Y_{ZH}}{2.86Y_{ZH}} \cdot r_3 - \frac{1 - Y_{ZH}}{2.86Y_{ZH}} \cdot r_4 + \frac{1}{Y_{ZA}} \cdot r_5 + \frac{1}{Y_{ZA}} \cdot r_6 \quad (9)$$

$$\frac{dN_{BP}}{dt} = (f_{ZN} - f_{ZE} \cdot f_{ZNE}) \cdot r_7 + (f_{ZN} - f_{ZE} \cdot f_{ZNE}) \cdot r_8 + (f_{ZN} - f_{ZE} \cdot f_{ZNE}) \cdot r_9 + (f_{ZN} - f_{ZE} \cdot f_{ZNE}) \cdot r_{10} - r_{13} \quad (10)$$

$$\frac{dN_{BS}}{dt} = -r_{11} + r_{13} \quad (11)$$

$$\frac{dS_{O2}}{dt} = -\frac{1 - Y_{ZH}}{Y_{ZH}} \cdot r_1 - \frac{1 - Y_{ZH}}{Y_{ZH}} \cdot r_2 - \frac{4.57 - Y_{ZA}}{Y_{ZA}} \cdot r_5 - \frac{4.57 - Y_{ZA}}{Y_{ZA}} \cdot r_6 + r_{14} \quad (12)$$

The values of relative constants for the established SDM are shown in Table 4. The flow conditions and reaeration effects are shown in Table 5. The equation set from Equation (1) to Equation (12) formed an ordinary differential equation (ODE) system. The set of ODEs was then solved simultaneously using the subroutine (SB) of the fourth-order Runge–Kutta algorithm (RK4) [22]. The flow chart for the computer program is shown in Figure 2.

3.4. OURBE to Calculate Sensitive Constants and Initial Biomass

In the model, there were many kinetic constants. The oxygen uptake rate batch experiments (OURBE) adopted from our previous studies [23–27] were used to measure the sensitive kinetic constants including maximum specific growth rate for heterotrophs, organism decay rate for heterotrophs, maximum specific growth rate for autotrophs, organism decay rate for autotrophs, and initial biomass of heterotrophs (Z_H) and autotrophs (Z_A).

The OURBE equipment consisted of several tanks of fixed height and volume and magnetic stirrers for agitation and aeration. Highly stable oxygen meters connected to the data processor were adopted to measure DO. Since the OURBE equipment was sealed and airtight, the actual respiration rate of microorganisms at any time did not depend on oxygen input into OURBE. The actual oxygen uptake rate (OUR) values could be measured using the DO values. A certain amount of biofilm was sampled from the PSP and added into the OURBE equipment. Substrates containing glucose, NH_4SO_4 , and KH_2PO_4 were added, resulting in a total volume of 1000 mL in the OURBE equipment, in which the pH value was controlled at 7. The OURBE equipment was periodically aerated to measure OUR. Furthermore, the kinetic constants and initial biomass of Z_H and Z_A could be measured [23–27].

For those constants that are nearly fixed values in domestic sewage, the default values from GDM and previous studies were used, as shown in Tables 4 and 5 [5,6,11–14].

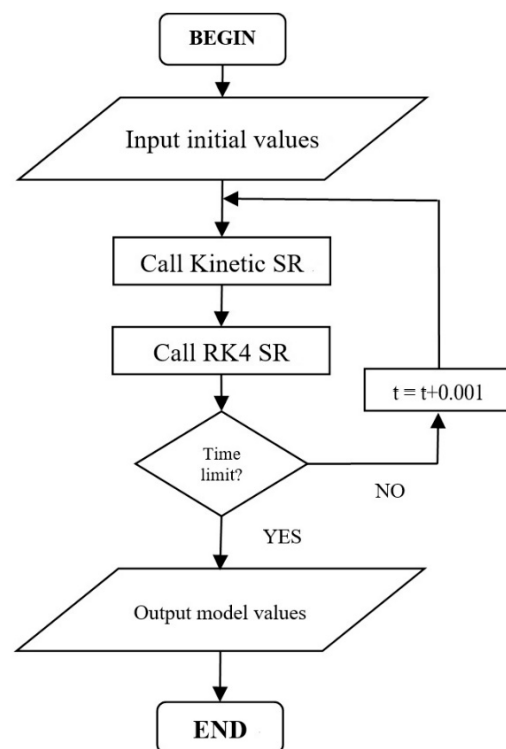


Figure 2. Computer program flow chart.

Table 4. Constant values.

Symbol	Definition	Value	Unit
μ_{ZH}	Maximum specific growth rate for heterotrophs	6	day^{-1}
b_{ZH}	Organism decay rate for heterotrophs	0.62	day^{-1}
Y_{ZH}	Yield for heterotrophs	0.67	$\text{g COD g}^{-1} \text{COD}$
$K_{O,ZH}$	DO half-saturation constant for heterotrophs	0.2	$\text{g O}_2 \text{ m}^{-3}$
$K_{S,ZH}$	Half-saturation constant for heterotrophic growth	20	g COD m^{-3}
K_{NO_3}	Nitrate half-saturation constant for denitrifying heterotrophs	0.5	$\text{g NO}_3\text{-N m}^{-3}$
η_{GRO}	Anoxic growth factor for μ_{ZH}	0.8	
μ_{ZA}	Maximum specific growth rate for autotrophs	0.8	day^{-1}
b_{ZA}	Organism decay rate for autotrophs	0.5	day^{-1}
Y_{ZA}	Yield for autotrophs	0.24	$\text{g COD g}^{-1} \text{COD}$
$K_{O,ZA}$	DO half-saturation constant for autotrophs	0.4	$\text{g O}_2 \text{ m}^{-3}$
K_{NH_3}	Half-saturation constant for autotrophic growth	1.0	$\text{g NH}_3\text{-N m}^{-3}$
K_{H}	Maximum specific hydrolysis rate	3	day^{-1}
K_{X}	Half-Saturation constant for hydrolysis	0.03	g COD m^{-3}
η_{h}	Anoxic factor for hydrolysis	0.4	
K_{R}	Ammonification rate	0.08	day^{-1}
f_{ZN}	Nitrogen content of active mass	0.086	
f_{ZNE}	Nitrogen content of endogenous mass	0.06	
f_{ZE}	Fraction of active mass remaining as endogenous residue	0.08	
ϵ	Efficiency constant in the biofilm	0.6	
θ_{W}	Temperature constant in the water phase	1.07	
θ_{F}	Temperature constant in the biofilm	1.03	

Table 5. Flow conditions and reaeration effect.

Symbol	Definition	Value	Unit
D_H	Hydraulic mean depth	0.15	m
F_R	Froude number = $V_M(g D_H)^{-0.5}$	Calculated	–
K_{La}	Overall oxygen transfer constant	Calculated	day ⁻¹
g	Gravity acceleration	9.81	m s ⁻²
$S_{O_2,SAT}$	Oxygen saturation concentration at T °C		g O ₂ m ⁻³
SLOP	Slope of sewer pipe	0.01	mm ⁻¹
T	Temperature	20	°C
V_M	Mean flow velocity	0.6	m s ⁻¹
θ_R	Temperature constant for reaeration	1.024	–

4. Results and Discussions

4.1. Experimental Results

In the PSP experiment, the volatile suspended solids (VSS) in the water phase were nearly 1.0 mg L⁻¹, so the Z_{HW} concentration was considered to be 1.0 mg L⁻¹. The autotrophs' biomass could not be easily measured using OURBE because of their low concentration, so Z_{AW} was considered to be 0.0 mg L⁻¹. The values of Z_{HF} and Z_{AF} were approximately 400.0 and 0.1 mg L⁻¹ in accordance with OURBE. These values were close to those in our previous in situ survey [28]. The Standard Methods [29] were adopted to measure the concentrations of other compounds. Nitrogen compound concentrations (N_{BP} , N_{SP} , N_{H_3} , and N_{O_3}) ranged from 2.0 to 30.1 mg L⁻¹. According to the PSP experiments, the initial OV_s for Z_{HW} , Z_{HF} , Z_{AW} , Z_{AF} , Z_E , S_{ENM} , S_{BCS} , N_{BP} , N_{BS} , N_{H_3} , N_{O_3} , and S_{O_2} were 1.0, 400.0, 0.0, 0.1, 1.0, 134.0, 281.0, 8.0, 30.1, 25.4, 2.0, and 6.2 mg L⁻¹, respectively. The OV_s of different compounds at various flowing times are shown in Figure 3.

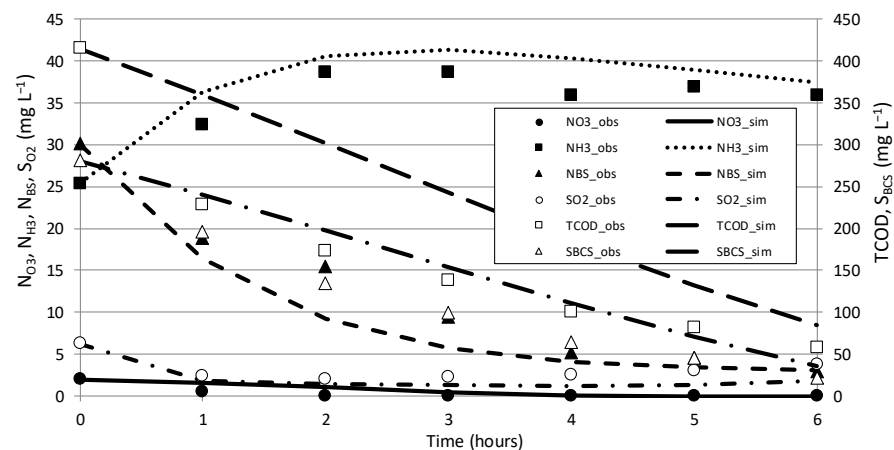


Figure 3. The OV_s of different compounds.

4.2. Model Validation

To verify the consistency between the SV_s and OV_s of different compounds in the water phase, the coefficient of determination (R^2) and correlation coefficient (R) were used as follows [30]:

$$R^2 = \frac{\sum_{i=1}^n (sv_i - \overline{sv})^2}{\sum_{i=1}^n (sv_i - sv_i)^2 + \sum_{i=1}^n (sv_i - \overline{sv})^2} \tag{13}$$

$$R = \frac{\sum_{i=1}^n (sv_i - \overline{sv})(ov_i - \overline{ov})}{\sqrt{\sum_{i=1}^n (sv_i - \overline{sv})^2 \sum_{i=1}^n (ov_i - \overline{ov})^2}} \tag{14}$$

where R^2 is the coefficient of determination, R is the correlation coefficient, sv is the SV, \overline{sv} is the mean SV, ov is the OV, \overline{ov} is the mean OV, and n is the number of concentrations. R^2 is used to explain how differences in OV can be explained by the difference in SV. It is represented as a value between 0.0 and 1.0. If the R^2 value is higher than 0.7, this value is generally considered as having a strong effect [30]. R is used to calculate the strength of the linear relationship between SV and OV. A value of R between 0.7 and 1.0 indicates a highly positive linear relationship. In this study, R^2 and R were used to justify whether SV and OV were consistent or not, providing a measure of how well OVs were replicated by the SDM model.

Figure 2 also shows the consistency between the SVs and OVs of selected compounds in the water phase. The R^2 values between SVs and OVs for S_{BCS} , N_{O_3} , N_{H_3} , N_{SP} , and S_{O_2} were 0.83, 0.70, 0.87, 0.91, and 0.73, respectively. The R values for those were 0.97, 0.81, 0.91, 0.97, and 0.93, respectively. These R^2 and R were greater than 0.7 and 0.81, respectively. According to the study proposed by Moore et al. [30], the SVs and OVs of the selected compounds were highly consistent.

4.3. RR of Z_{HW}

Since the established model was validated, the RRs of different compounds at different flowing times could be calculated. Figure 4 shows the calculated RRs within 6 h.

According to Equation (1), Z_{HW} would grow because of r_1 (aerobic growth of Z_{HW} in the water phase) and r_3 (anoxic growth of Z_{HW} in the water phase), and decay because of r_7 (organism decay of Z_{HW} in the water phase). In the simulation proposed by Tanaka and Hvitved-Jacobsen [31], Z_{HW} would grow from 32.0 to 35.0 mg L⁻¹ within the initial 4 h, revealing positive RRs.

In Figure 4a, the RR for Z_{HW} was 0.155 mg L⁻¹ h⁻¹ at the initial time, began to increase before the 3rd hour, and reached its highest value of 0.202 mg L⁻¹ h⁻¹ at the 3rd–4th hour, afterward the RR decreased gradually to a value of 0.176 mg L⁻¹ h⁻¹ at the 6th hour.

Before the 3rd hour, the r_1 (aerobic growth of Z_{HW} in the water phase) and r_3 (anoxic growth of Z_{HW} in the water phase) with positive signs were high because of high S_{BCS} as shown in Figure 3. Therefore, the sum for the growth rate of Z_{HW} ($r_1 + r_3$) was greater than r_7 (organism decay of Z_{HW} in the water phase) and the RRs began to increase before the 3rd hour. After the 4th hour, the sum for the growth rate of Z_{HW} ($r_1 + r_3$) was less than r_7 because the sum for the growth rate of Z_{HW} became lower. Therefore, the RRs revealed a decreasing trend after the 4th hour.

4.4. RR of Z_{HF}

According to Equation (2), Z_{HF} would grow because of r_2 (aerobic growth of Z_{HF} in the biofilm) and r_4 (anoxic growth of Z_{HF} in the biofilm), and decay because of r_8 (organism decay of Z_{HF} in the biofilm). According to a study by Nielsen et al. [32], the biofilms grew linearly at an average rate of 0.2 mm day⁻¹ thickness during a series of experiments, revealing positive RRs.

In Figure 4b, the rates of Z_{HF} were 31.2 mg L⁻¹ h⁻¹ at the initial time, began to increase before the 2nd hour, and reached the highest value of 32.3 mg L⁻¹ h⁻¹ at the 2nd hour, afterward, the RR decreased gradually to a value of 19.9 mg L⁻¹ h⁻¹ at the 6th hour.

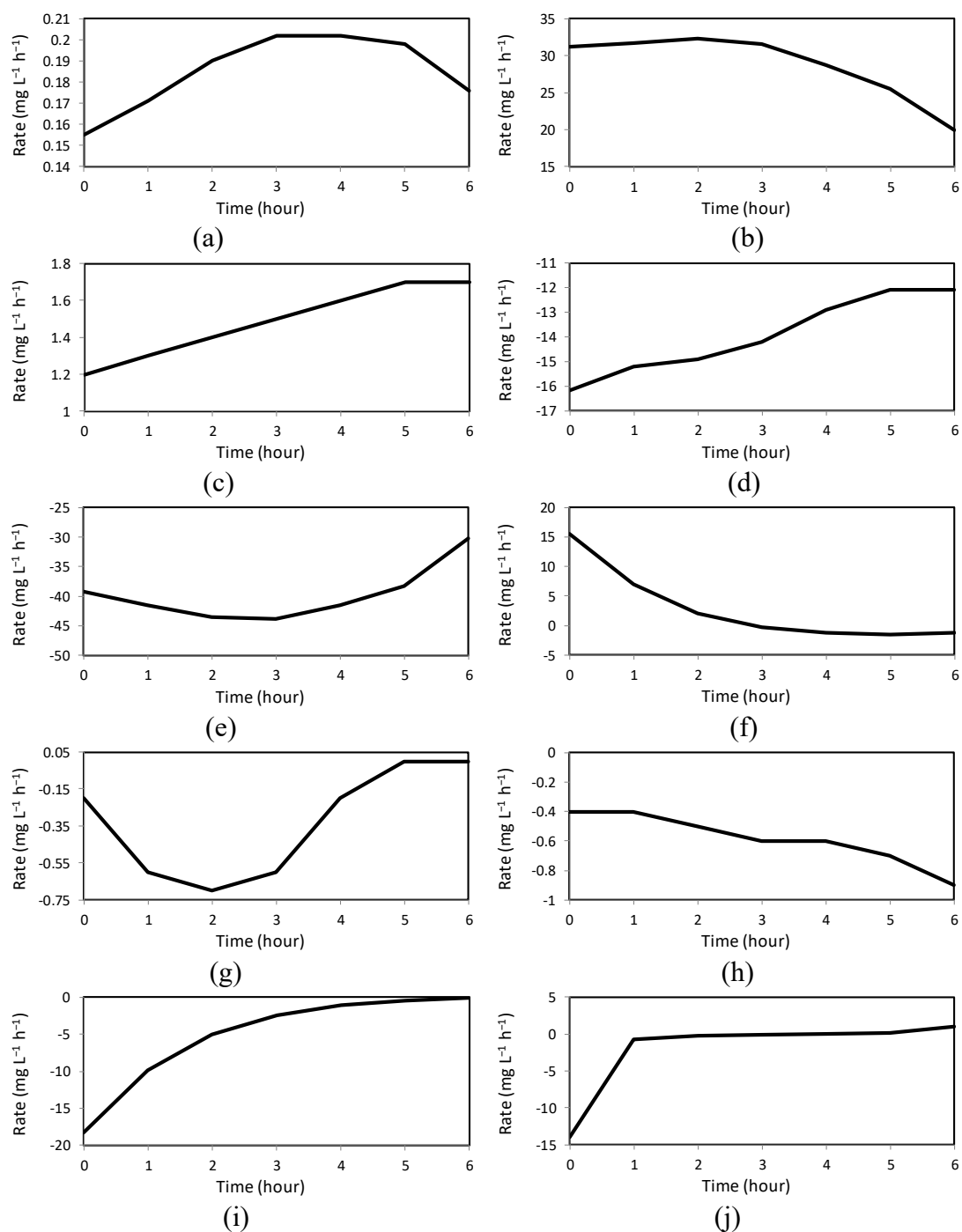


Figure 4. The RRs of different compounds at different flowing times. (a) Z_{HW} , (b) Z_{HF} , (c) Z_E , (d) S_{ENM} , (e) S_{BCS} , (f) N_{H3} , (g) NO_3 , (h) N_{BP} , (i) N_{BS} , and (j) SO_2 .

Before the 2nd hour, the r_2 (aerobic growth of Z_{HF} in the biofilm) and r_4 (anoxic growth of Z_{HF} in the biofilm) with positive signs were high because of high S_{BCS} as shown in Figure 3. Therefore, the sum for the growth rate of Z_{HF} ($r_2 + r_4$) was greater than r_8 (organism decay of Z_{HF} in the biofilm) and the RRs began to increase before the 2nd hour. After the 2nd hour, the sum for the growth rate of Z_{HF} ($r_2 + r_4$) was less than r_8 because the sum for the growth rate of Z_{HF} became lower. Thus, the RRs revealed a decreasing trend after the 2nd hour.

4.5. RRs of Z_{AW} and Z_{AF}

According to Equation (3), Z_{AW} would grow because of r_5 (aerobic growth of Z_{AW} in the water phase) and decay because of r_9 (organism decay of Z_{AW} in the water phase). According to Equation (4), Z_{AF} would grow because of r_6 (aerobic growth of Z_{AF} in the biofilm) and decay because of r_{10} . In the experiment, the organism biomass of the autotrophs in the water phase was ignored. The value of Z_{AF} was about 0.1 mg L^{-1} according to OURBE. The calculation indicated that the RRs of Z_{AW} and Z_{AF} were almost zero.

4.6. RR of Z_E

According to Equation (5), Z_E would increase because of r_7 (organism decay of Z_{HW} in the water phase), r_8 (organism decay of Z_{HF} in the biofilm), r_9 (organism decay of Z_{AW} in the water phase), and r_{10} (organism decay of Z_{AF} in the biofilm).

In Figure 4c, the RR of Z_E was $1.2 \text{ mg L}^{-1} \text{ h}^{-1}$ at the initial time, began to increase, and reached the highest value of $1.7 \text{ mg L}^{-1} \text{ h}^{-1}$ at the 5th hour, afterward, the RR remained fixed at the value $1.7 \text{ mg L}^{-1} \text{ h}^{-1}$ at the 6th hour.

Before the 5th hour, the biomass of Z_{HW} , Z_{HF} , Z_{AW} , and Z_{AF} in r_7 (organism decay of Z_{HW} in the water phase), r_8 (organism decay of Z_{HF} in the biofilm), r_9 (organism decay of Z_{AW} in the water phase), and r_{10} (organism decay of Z_{AF} in the biofilm) increased continuously. Thus, the RR of Z_E continuously increased before the 5th hour. After the 5th hour, the biomass for the organisms was more stable, so the RR remained fixed at the value of $1.7 \text{ mg L}^{-1} \text{ h}^{-1}$ at the 6th hour.

4.7. RR of S_{ENM}

According to Equation (6), S_{ENM} would be supplied because of r_7 (organism decay of Z_{HW} in the water phase), r_8 (organism decay of Z_{HF} in the biofilm), r_9 (organism decay of Z_{AW} in the water phase), and r_{10} (organism decay of Z_{AF} in the biofilm), and consumed because of r_{12} (hydrolysis of S_{ENM}). According to the simulation carried out by Vollertsen et al. [33], in which the maximum specific hydrolysis rate for S_{ENM} was 4.0 day^{-1} , the S_{ENM} was 40 mg L^{-1} at the 0th km and 28 mg L^{-1} at the 20th km, revealing significant biodegradation and negative RRs.

In Figure 4d, the RR of S_{ENM} was $-16.2 \text{ mg L}^{-1} \text{ h}^{-1}$ at the initial time and increased gradually to a value of $-12.1 \text{ mg L}^{-1} \text{ h}^{-1}$ at the 6th hour. During the whole experimental time of 6 h, the r_7 (organism decay of Z_{HW} in the water phase), r_8 (organism decay of Z_{HF} in the biofilm), r_9 (organism decay of Z_{AW} in the water phase), and r_{10} (organism decay of Z_{AF} in the biofilm) with positive signs were low, but r_{12} (hydrolysis of S_{ENM}) with a negative sign was relatively high. However, r_{12} became lower because of decreasing S_{ENM} , so the RR of S_{ENM} increased gradually. It indicated that the supply rate of S_{ENM} was lower than the consumption rate in the experiment.

4.8. RR of S_{BCS}

According to Equation (7), S_{BCS} would be consumed because of r_1 (aerobic growth of Z_{HW} in the water phase), r_2 (aerobic growth of Z_{HF} in the biofilm), r_3 (anoxic growth of Z_{HW} in the water phase), and r_4 (anoxic growth of Z_{HF} in the biofilm), and supplied because of r_{12} (hydrolysis of S_{ENM}). According to previous studies reported by Raunkjær et al. [34], the removal rate of S_{BCS} (acetate) was $4.13 \text{ g m}^{-2} \text{ h}^{-1}$ and $1.98 \text{ g m}^{-2} \text{ h}^{-1}$ under low-loaded and high-loaded conditions, respectively, revealing significant biodegradation. In the simulation proposed by Vollertsen et al. [33], the S_{BCS} was 30 mg L^{-1} at the 0th km and 3 mg L^{-1} at the 20th km, revealing significant biodegradation and negative RRs.

In Figure 4e, the RR of S_{BCS} was $-39.2 \text{ mg L}^{-1} \text{ h}^{-1}$ at the initial time, began to decrease before the 3rd hour and reached the lowest value of $-43.9 \text{ mg L}^{-1} \text{ h}^{-1}$ at the 3rd hour, afterward the RR increased gradually to a value of $-30.2 \text{ mg L}^{-1} \text{ h}^{-1}$ at the 6th hour.

Before the 3rd hour, the r_1 (aerobic growth of Z_{HW} in the water phase), r_2 (aerobic growth of Z_{HF} in the biofilm), r_3 (anoxic growth of Z_{HW} in the water phase), and r_4 (anoxic growth of Z_{HF} in the biofilm) with negative signs were high because of high S_{BCS} , but r_{12}

(hydrolysis of S_{ENM}) with a positive sign was relatively low. After the 3rd hour, the sum for consumption rate of S_{BCS} ($r_1 + r_2 + r_3 + r_4$) became lower because of low S_{BCS} . So the RRs revealed an increasing trend after the 3rd hour. The RR of S_{BCS} was highly negative at the initial time and final time. It indicated that the supply rate of S_{BCS} was lower than the consumption rate in the experiment.

4.9. RR of N_{H3}

According to Equation (8), N_{H3} would be consumed because of r_1 (aerobic growth of Z_{HW} in the water phase), r_2 (aerobic growth of Z_{HF} in the biofilm), r_3 (anoxic growth of Z_{HW} in the water phase), r_4 (anoxic growth of Z_{HF} in the biofilm), r_5 (aerobic growth of Z_{AW} in the water phase), and r_6 (aerobic growth of Z_{AF} in the biofilm), and supplied because of r_{11} (ammonification of N_{BS}). In a study by Marjaka et al. [35], the removal of dissolved organic carbon and nitrogen in a USP with a fabricated porous ceramic bed was investigated. When N_{H3} was used as the nitrogen source, and air was supplied through the aerator, 56% of the initial N_{H3} was removed within 180 min. On the other hand, the value was about 38% when aeration was not applied. In their nitrification test, the RR of N_{H3} was negative. But in our study, the RR of N_{H3} was positive because of the hydrolysis of organic nitrogen.

In Figure 4f, the RR of N_{H3} was $15.5 \text{ mg L}^{-1} \text{ h}^{-1}$ at the initial time, began to decrease before the 5th hour and reached the lowest value of $-1.6 \text{ mg L}^{-1} \text{ h}^{-1}$ at the 5th hour, afterward, the RR increased slightly to a value of $-1.2 \text{ mg L}^{-1} \text{ h}^{-1}$ at the 6th hour.

Before the 5th hour, the r_1 (aerobic growth of Z_{HW} in the water phase), r_2 (aerobic growth of Z_{HF} in the biofilm), r_3 (anoxic growth of Z_{HW} in the water phase), r_4 (anoxic growth of Z_{HF} in the biofilm), r_5 (aerobic growth of Z_{AW} in the water phase), and r_6 (aerobic growth of Z_{AF} in the biofilm) with negative signs decreased highly because of high N_{H3} , but r_{11} (ammonification of N_{BS}) with a positive sign increased slightly. Thus, N_{H3} decreased before the 5th hour.

It indicated that the supply rate of N_{H3} was greater than the consumption rate at the initial time, but the supply rate was smaller than the consumption rate from 3rd hour in the experiment. The RR of N_{H3} could be also regarded as the nitrification rate. Since the supply rate of N_{H3} was greater than the consumption rate, the nitrification rate was not obvious. This is consistent with the results proposed by Shoji et al. [36], Liang et al. [37], and our previous in-situ study [28].

4.10. RR of N_{O3}

According to Equation (9), N_{O3} would be consumed because of r_3 (anoxic growth of Z_{HW} in the water phase) and r_4 (anoxic growth of Z_{HF} in the biofilm), and supplied because of r_5 (aerobic growth of Z_{AW} in the water phase) and r_6 (aerobic growth of Z_{AH} in the biofilm). In the study proposed by Marjaka et al. [35], nitrite and nitrate concentrations in the nitrification test were low, indicating that the conversion of nitrite and nitrate to nitrogen gas by denitrification might undergo; therefore, the RR of N_{O3} was negative. In the experiments carried out by Æsøy et al. [38], the denitrification rate of $3.5\text{--}4.3 \text{ g NO}_3\text{-N m}^{-2} \text{ day}^{-1}$ was observed in the PSP. This indicated the RR of N_{O3} was negative in the PSP.

In Figure 4g, the RR of N_{O3} was $-0.2 \text{ mg L}^{-1} \text{ h}^{-1}$ at the initial time, began to decrease before the 2nd hour, reached the lowest value of $-0.7 \text{ mg L}^{-1} \text{ h}^{-1}$ at the 2nd hour, afterward the RR increased gradually to a value of $0.0 \text{ mg L}^{-1} \text{ h}^{-1}$ at the 6th hour.

Before the 2nd hour, the r_3 (anoxic growth of Z_{HW} in the water phase) and r_4 (anoxic growth of Z_{HF} in the biofilm) with negative signs decreased highly, but r_5 (aerobic growth of Z_{AW} in the water phase) and r_6 (aerobic growth of Z_{AH} in the biofilm) with positive signs increased slightly. Thus, the RR of N_{O3} decreased before the 2nd hour. After the 2nd hour, r_3 and r_4 became lower because of low N_{O3} . Therefore, the RRs revealed an increasing trend after the 2nd hour.

This indicated that the supply rate was smaller than the consumption rate in the experiment. The RR of N_{O3} could be also be regarded as the denitrification rate. Denitrification

did not occur obviously because of the low initial concentration and poor denitrification activity. This is consistent with the results proposed by Shoji et al. [36].

4.11. RR of N_{BP}

According to Equation (10), N_{BP} would be supplied because of r_7 (organism decay of Z_{HW} in the water phase), r_8 (organism decay of Z_{HF} in the biofilm), r_9 (organism decay of Z_{AW} in the water phase), and r_{10} (organism decay of Z_{AF} in the biofilm), and consumed because of r_{13} (hydrolysis of N_{BP}).

In Figure 4h, the RR of N_{BP} was $-0.4 \text{ mg L}^{-1} \text{ h}^{-1}$ at the initial time and decreased gradually to a value of $-0.9 \text{ mg L}^{-1} \text{ h}^{-1}$ at the 6th hour.

During the whole experimental time of 6 h, the r_7 (organism decay of Z_{HW} in the water phase), r_8 (organism decay of Z_{HF} in the biofilm), r_9 (organism decay of Z_{AW} in the water phase), and r_{10} (organism decay of Z_{AF} in the biofilm) with positive signs were low, but r_{13} (hydrolysis of N_{BP}) with a negative sign was relatively high. Therefore, the RR of N_{BP} decreased gradually to a value of $-0.9 \text{ mg L}^{-1} \text{ h}^{-1}$ at the 6th hour. This indicated that the supply rate of N_{BP} was smaller than the consumption rate in the experiment.

4.12. RR of N_{BS}

According to Equation (11), N_{BS} would be consumed because of r_{11} (ammonification of N_{BS}) and supplied because of r_{13} (hydrolysis of N_{BP}).

In Figure 4i, the RR of N_{BS} was $-18.3 \text{ mg L}^{-1} \text{ h}^{-1}$ at the initial time and increased gradually to a value of $-0.1 \text{ mg L}^{-1} \text{ h}^{-1}$ at the 6th hour. During the whole experimental time of 6 h, the r_{11} (ammonification of N_{BS}) with a negative sign was greater than r_{13} (hydrolysis of N_{BP}) with a positive sign. Thus, the RR of N_{BS} increased gradually. It indicated that the supply rate was smaller than the consumption rate in the experiment.

4.13. RR of S_{O_2}

According to Equation (12), S_{O_2} would be consumed because of r_1 (aerobic growth of Z_{HW} in the water phase), r_2 (aerobic growth of Z_{HF} in the biofilm), r_5 (aerobic growth of Z_{AW} in the water phase), and r_6 (aerobic growth of Z_{AF} in the biofilm), and supplied because of r_{14} (reaeration of oxygen) [39]. In a study by Marjaka et al. [35], the S_{O_2} value was decreased to 2.0 mg L^{-1} within the first 15 min, and then increased gradually to 6.0 mg L^{-1} when organic carbon was almost completely consumed. When no aeration was applied, the S_{O_2} concentration decreased to 0.0 mg L^{-1} within 30.0 min and an anaerobic condition was maintained until 120.0 min. Then S_{O_2} concentration gradually increased to 4.0 mg L^{-1} during the rest period.

In Figure 4j, the RR of S_{O_2} was $-14.0 \text{ mg L}^{-1} \text{ h}^{-1}$ at the initial time, $0.0 \text{ mg L}^{-1} \text{ h}^{-1}$ at the 4th hour, and $1.0 \text{ mg L}^{-1} \text{ h}^{-1}$ at the 6th hour, respectively.

According to Figure 3, S_{O_2} was 6.23 mg L^{-1} at the initial time, began to decrease to the lowest value of 1.98 mg L^{-1} at the 2nd hour, and then increased gradually to 3.76 mg L^{-1} at the 6th hour. Therefore, the r_1 (aerobic growth of Z_{HW} in the water phase), r_2 (aerobic growth of Z_{HF} in the biofilm), r_5 (aerobic growth of Z_{AW} in the water phase), and r_6 (aerobic growth of Z_{AF} in the biofilm) with negative signs were greater than r_{14} (reaeration of oxygen) with a positive sign before the 2nd hour. After the 2nd hour, r_{14} (reaeration of oxygen) was greater than the sum of r_1 , r_2 , r_5 , and r_6 . Thus, the RR of S_{O_2} increased gradually to a value of $1.0 \text{ mg L}^{-1} \text{ h}^{-1}$ at the 6th hour.

This indicated that the supply rate was smaller than the consumption rate before the 4th hour because of significant organism activity, and, subsequently, the supply rate was greater than the consumption rate after the 4th hour because of reaeration.

5. Conclusions

The SDM, an innovative use of combined models, was established to describe the reaction of several compounds in the PSP. The established model was validated by calculating the consistency between the SVs and OV_s of different compounds. R^2 and R were greater than 0.7 and 0.81, respectively, revealing that the SVs and OV_s of selected compounds were highly consistent. Therefore, the RRs of compounds in the PSP were calculated using the SDM.

For Z_{HW} and Z_{HF} , their growth rates were greater than the organism decay rates in the experiment. For Z_E , S_{ENM} , S_{BCS} , NO_3 , N_{BP} , and N_{BS} , their supply rate was smaller than the consumption rate in the experiment. For N_{H3} , the supply rate was greater than the consumption rate at the initial time, but the supply rate was smaller than the consumption rate from 3rd hour in the experiment. The supply rate of SO_2 was smaller than the consumption rate before the 4th hour because of significant microorganism activity, and, subsequently, the supply rate was greater than the consumption rate after the 4th hour because of reaeration. The kinetic constants and RREs in the SDM could be applied to predict the real-world situation.

6. Recommendations for Future Research

The results of this study not only provide an insight into the reaction rates of different compounds in the USP and an urban water network modeling reference for policymaking and regulation but also valuable data to help designers create more reasonable USP planning. However, in situ experiments in the USP are suggested to further explore the SDM in the future.

Author Contributions: Conceptualization, T.-Y.P. and T.-J.W.; methodology, T.-Y.P. and H.-M.L.; software, T.-Y.P.; validation, Y.-H.W., Y.-H.C., M.-H.T., H.T., Y.-X.S., W.-C.C., and Y.-P.L.; formal analysis, all authors; writing—original draft preparation, T.-Y.P.; writing—review and editing, H.-M.L. and T.-J.W. All authors have read and agreed to the published version of the manuscript.

Funding: This research received no external funding.

Institutional Review Board Statement: Not applicable.

Informed Consent Statement: Not applicable.

Data Availability Statement: Some data and models related to this study are available from the corresponding author upon reasonable request.

Acknowledgments: The authors are grateful to the Ministry of Science and Technology of R.O.C. for financial support under the grant number MOST 108-2221-E-142-003-MY2.

Conflicts of Interest: The authors declare no conflict of interest.

Nomenclature

Symbols

b_{ZA}	Organism decay rate for autotrophs (day^{-1})
b_{ZH}	Organism decay rate for heterotrophs (day^{-1})
D_H	Hydraulic mean depth (m)
F_R	Froude number
f_{ZE}	Fraction of active mass remaining as endogenous residue
f_{ZN}	Nitrogen content of active mass
f_{ZNE}	Nitrogen content of endogenous mass
g	Gravity acceleration (m s^{-2})
K_H	Maximum specific hydrolysis rate (day^{-1})
K_{NH3}	Half-saturation constant for autotrophic growth ($\text{gNH}_3\text{-Nm}^{-3}$)
K_{NO3}	Nitrate half-saturation constant for denitrifying heterotrophs ($\text{gNO}_3\text{-Nm}^{-3}$)
K_{La}	Overall oxygen transfer constant (day^{-1})

$K_{O,ZH}$	DO half-saturation constant for heterotrophs (gO_2m^{-3})
$K_{O,ZA}$	DO half-saturation constant for autotrophs (gO_2m^{-3})
K_R	Ammonification rate (day^{-1})
$K_{S,ZH}$	Half-saturation constant for heterotrophic growth (gCODm^{-3})
K_X	Half-saturation constant for hydrolysis (gCODm^{-3})
ov	Observation value
\bar{ov}	Mean observation value
N_{BP}	Particulate biodegradable organic nitrogen (g OrgNm^{-3})
N_{BS}	Soluble biodegradable organic nitrogen (g OrgNm^{-3})
N_{H3}	Ammonia-nitrogen ($\text{g NH}_3\text{m}^{-3}$)
N_{O3}	Nitrate and nitrite nitrogen ($\text{g NO}_2^- + \text{NO}_3^- \text{m}^{-3}$)
R	Correlation coefficient
R^2	Coefficient of determination
r_1	Aerobic growth of Z_{HW} in the water phase
r_2	Aerobic growth of Z_{HF} in the biofilm
r_3	Anoxic growth of Z_{HW} in the water phase
r_4	Anoxic growth of Z_{HF} in the biofilm
r_5	Aerobic growth of Z_{AW} in the water phase
r_6	Aerobic growth of Z_{AF} in the biofilm
r_7	Organism decay of Z_{HW} in the water phase
r_8	Organism decay of Z_{HF} in the biofilm
r_9	Organism decay of Z_{AW} in the water phase
r_{10}	Organism decay of Z_{AF} in the biofilm
r_{11}	Ammonification of N_{BS}
r_{12}	Hydrolysis of S_{ENM}
r_{13}	Hydrolysis of N_{BP}
r_{14}	Reaeration of oxygen
S_{BCS}	Readily biodegradable “complex” substrate (g CODm^{-3})
S_{ENM}	Enmeshed slowly biodegradable substrates (g CODm^{-3})
S_{LOP}	Slope of sewer pipe (mm^{-1})
S_{O2}	Oxygen ($\text{g O}_2\text{m}^{-3}$)
$S_{O2,SAT}$	Oxygen saturation concentration at T °C ($\text{g O}_2\text{m}^{-3}$)
sv	Simulation value
\bar{sv}	Mean simulation value
T	Temperature (°C)
V_M	Mean flow velocity (m s^{-1})
Y_{ZA}	Yield for autotrophs ($\text{gCOD g}^{-1}\text{COD}$)
Y_{ZH}	Yield for heterotrophs ($\text{gCOD g}^{-1}\text{COD}$)
Z_A	Active autotrophic biomass (g CODm^{-3})
Z_{AF}	Active autotrophic biomass in the biofilm (g CODm^{-3})
Z_{AW}	Active autotrophic biomass in the water phase (g CODm^{-3})
Z_E	Endogenous mass (g CODm^{-3})
Z_H	Active heterotrophic biomass (g CODm^{-3})
Z_{HF}	Active heterotrophic biomass in the biofilm (g CODm^{-3})
Z_{HW}	Active heterotrophic biomass in the water phase (g CODm^{-3})
ϵ	Efficiency constant in the biofilm
η_{GRO}	Anoxic growth factor for μ_{ZH}
η_h	Anoxic factor for hydrolysis
θ_F	Temperature constant in the biofilm
θ_R	Temperature constant for reaeration
θ_W	Temperature constant in the water phase
μ_{ZA}	Maximum specific growth rate for autotrophs (day^{-1})
μ_{ZH}	Maximum specific growth rate for heterotrophs (day^{-1})
Abbreviations	
ASM	Activated Sludge Model
COD	Chemical oxygen demand

DO	Dissolved oxygen
GDM	General Dynamic Model
HCSS	Highly concentrated synthesis sewage
ODE	Ordinary differential equation
OUR	Oxygen uptake rate
OURBE	Oxygen uptake rate batch experiment
OV	Observation values
RK4	The fourth-order Runge-Kutta algorithm
PSP	Pilot sewer pipe
RR	Reaction rate
RRE	Reaction rate equation
SB	Subroutine
SDM	Sewer dynamic model
STP	Sewage treatment plant
SV	Simulation value
USP	Urban sewer pipe
VSS	Volatile suspended solids

References

1. Tung, Y.T.; Pai, T.Y. Water management for agriculture, energy and social security in Taiwan. *Clean (Weinh)* **2015**, *43*, 627–632. [[CrossRef](#)]
2. Jiang, F.; Leung, D.H.; Li, S.; Chen, G.-H.; Okabe, S.; van Loosdrecht, M.C.M. A biofilm model for prediction of pollutant transformation in sewers. *Water Res.* **2009**, *43*, 3187–3198. [[CrossRef](#)]
3. Gao, J.; Li, J.; Jiang, G.; Shypanski, A.H.; Nieradzick, L.M.; Yuan, Z.; Mueller, J.F.; Ort, C.; Thai, P.K. Systematic evaluation of biomarker stability in pilot scale sewer pipes. *Water Res.* **2019**, *151*, 447–455. [[CrossRef](#)]
4. Nielsen, A.H.; Vollertsen, J. Model parameters for aerobic biological sulfide oxidation in sewer wastewater. *Water* **2021**, *13*, 981. [[CrossRef](#)]
5. Pai, T.Y.; Shyu, G.S.; Chen, L.; Lo, H.M.; Chang, D.H.; Lai, W.J.; Yang, P.Y.; Chen, C.Y.; Liao, Y.C.; Tseng, S.C. Modelling transportation and transformation of nitrogen compounds at different influent concentrations in sewer pipe. *Appl. Math. Model.* **2013**, *37*, 1553–1563. [[CrossRef](#)]
6. Pai, T.Y.; Wang, S.C.; Lo, H.M.; Chen, L.; Wan, T.J.; Lin, M.R.; Lin, C.Y.; Yang, P.Y.; Lai, W.J.; Wang, Y.H.; et al. A simulation of sewer biodeterioration by analysis of different components with a model approach. *Int. Biodeterior. Biodegrad.* **2017**, *125*, 37–44. [[CrossRef](#)]
7. Butler, D.; Friedler, E.; Gatt, K. Characterising the quantity and quality of domestic wastewater inflows. *Water Sci. Technol.* **1995**, *31*, 13–24. [[CrossRef](#)]
8. Short, M.D.; Peirson, W.L.; Peters, G.M.; Cox, R.J. Managing adaptation of urban water systems in a changing climate. *Water Resour. Manag.* **2012**, *26*, 1953–1981. [[CrossRef](#)]
9. Short, M.D.; Daikeler, A.; Peters, G.M.; Mann, K.; Ashbolt, N.J.; Stuetz, R.M.; Peirson, W.L. Municipal gravity sewers: An unrecognised source of nitrous oxide. *Sci. Total Environ.* **2014**, *468–469*, 211–218. [[CrossRef](#)]
10. Van de Walle, J.L.; Goetz, G.W.; Huse, S.M.; Morrison, H.G.; Sogin, M.L.; Hoffmann, R.G.; Yan, K.; McLellan, S.L. Acinetobacter, Aeromonas and Trichococcus populations dominate the microbial community within urban sewer infrastructure. *Environ. Microbiol.* **2012**, *14*, 2538–2552. [[CrossRef](#)] [[PubMed](#)]
11. Henze, M.; Gujer, W.; Mino, T.; van Loosdrecht, M.C.M. *Activated Sludge Models: ASM1, ASM2, ASM2d and ASM3*; International Water Association: London, UK, 2000.
12. Hvitved-Jacobsen, T.; Vollertsen, J.; Nielsen, P.H. A process and model concept for microbial wastewater transformations in gravity sewers. *Water Sci. Technol.* **1998**, *37*, 233–241. [[CrossRef](#)]
13. Hvitved-Jacobsen, T.; Vollertsen, J.; Tanaka, N. Wastewater quality changes during transport in sewers—an integrated aerobic and anaerobic model concept for carbon and sulfur microbial transformations. *Water Sci. Technol.* **1998**, *38*, 257–264. [[CrossRef](#)]
14. Vollertsen, J.; Hvitved-Jacobsen, T. Aerobic microbial transformations of resuspended sediments in combined sewers—a conceptual model. *Water Sci. Technol.* **1998**, *37*, 69–76. [[CrossRef](#)]
15. Dittmer, U.; Bachmann-Machnik, A.; Launay, M.A. Impact of combined sewer systems on the quality of urban streams: Frequency and duration of elevated micropollutant concentrations. *Water* **2020**, *12*, 850. [[CrossRef](#)]
16. Langeveld, J.; van Daal, P.; Schilperoord, R.; Nopens, I.; Flameling, T.; Weijers, S. Empirical sewer water quality model for generating influent data for WWTP modelling. *Water* **2017**, *9*, 491. [[CrossRef](#)]
17. Pai, T.Y.; Chuang, S.H.; Tsai, Y.P.; Ouyang, C.F. Modelling a combined anaerobic/anoxic oxide and rotating biological contactors process under dissolved oxygen variation by using an activated sludge-biofilm hybrid model. *J. Environ. Eng.* **2004**, *130*, 1433–1441. [[CrossRef](#)]
18. Pai, T.Y.; Ouyang, C.F.; Su, J.L.; Leu, H.G. Modelling the steady-state effluent characteristics of the TNCU process under different return mixed liquid. *Appl. Math. Model.* **2001**, *25*, 1025–1038. [[CrossRef](#)]

19. Pai, T.Y.; Tsai, Y.P.; Chou, Y.J.; Chang, H.Y.; Leu, H.G.; Ouyang, C.F. Microbial kinetic analysis of three different types of EBNR process. *Chemosphere* **2004**, *55*, 109–118. [[CrossRef](#)] [[PubMed](#)]
20. Pai, T.Y. Modeling nitrite and nitrate variations in A2O process under different return oxalic mixed liquid using an extended model. *Process. Biochem.* **2007**, *42*, 978–987. [[CrossRef](#)]
21. Pai, T.Y.; Chang, H.Y.; Wan, T.J.; Chuang, S.H.; Tsai, Y.P. Using an extended activated sludge model to simulate nitrite and nitrate variations in TNCU2 process. *Appl. Math. Model.* **2009**, *33*, 4259–4268. [[CrossRef](#)]
22. Gerald, C.F.; Wheatley, P.O. *Applied Numerical Analysis*, 4th ed.; Addison-Wesley Publishing Company Inc.: New York, NY, USA, 1989.
23. Pai, T.Y.; Wang, S.C.; Lo, H.M.; Chiang, C.F.; Liu, M.H.; Chiou, R.J.; Chen, W.Y.; Hung, P.S.; Liao, W.C.; Leu, H.G. Novel modeling concept for evaluating the effects of cadmium and copper on heterotrophic growth and lysis rates in activated sludge process. *J. Hazard. Mater.* **2009**, *166*, 200–206. [[CrossRef](#)] [[PubMed](#)]
24. Pai, T.Y.; Wang, S.C.; Lin, C.Y.; Liao, W.C.; Chu, H.H.; Lin, T.S.; Liu, C.C.; Lin, S.W. Two types of organophosphate pesticides and their combined effects on heterotrophic growth rates in activated sludge process. *J. Chem. Technol. Biotechnol.* **2009**, *84*, 1773–1779. [[CrossRef](#)]
25. Pai, T.Y.; Wan, T.J.; Tsai, Y.P.; Tzeng, C.J.; Chu, H.H.; Tsai, Y.S.; Lin, C.Y. Effect of sludge retention time on nitrifiers' biomass and kinetics in an anaerobic/oxic process. *Clean* **2010**, *38*, 167–172. [[CrossRef](#)]
26. Pai, T.Y.; Chiou, R.J.; Tzeng, C.J.; Lin, T.S.; Yeh, S.C.; Sung, P.J.; Tseng, C.H.; Tsai, C.H.; Tsai, Y.S.; Hsu, W.J.; et al. Variation of biomass and kinetic parameter for nitrifying species in TNCU3 process at different aerobic hydraulic retention time. *World J. Microbiol. Biotechnol.* **2010**, *26*, 589–597. [[CrossRef](#)]
27. Pai, T.Y.; Lo, H.M.; Wan, T.J.; Wang, S.C.; Yang, P.Y.; Huang, Y.T. Behaviors of biomass and kinetic parameter for nitrifying species in A2O process at different sludge retention time. *Appl. Biochem. Biotechnol.* **2014**, *174*, 2875–2885. [[CrossRef](#)] [[PubMed](#)]
28. Pai, T.Y.; Chen, C.L.; Chung, H.; Ho, H.H.; Shiu, T.W. Monitoring and assessing variation of sewage quality and microbial functional groups in a trunk sewer line. *Environ. Monit. Assess.* **2010**, *171*, 551–560. [[CrossRef](#)]
29. APHA; AWWA; WEF. *Standard Methods for the Examination of Water and Wastewater*, 20th ed.; American Public Health Association, American Water Works Association and Water Environment Federation: Washington, DC, USA, 1998.
30. Moore, D.S.; Notz, W.I.; Flinger, M.A. *The Basic Practice of Statistics*, 6th ed.; W.H. Freeman and Company: New York, NY, USA, 2013.
31. Tanaka, N.; Hvitved-Jacobsen, T. Transformations of wastewater organic matter in sewers under changing aerobic/anaerobic conditions. *Water Sci. Technol.* **1998**, *37*, 105–113. [[CrossRef](#)]
32. Nielsen, A.H.; Hvitved-Jacobsen, T.; Vollertsen, J. Kinetics and stoichiometry of sulfide oxidation by sewer biofilms. *Water Res.* **2005**, *39*, 4119–4125. [[CrossRef](#)] [[PubMed](#)]
33. Vollertsen, J.; Hvitved-Jacobsen, T.; McGregor, I.; Ashley, R. Aerobic microbial transformations of pipe and silt trap sediments from combined sewers. *Water Sci. Technol.* **1999**, *39*, 233–249. [[CrossRef](#)]
34. Raunkjær, K.; Nielsen, P.H.; Hvitved-Jacobsen, T. Acetate removal in sewer biofilms under aerobic conditions. *Water Res.* **1997**, *31*, 2727–2736. [[CrossRef](#)]
35. Marjaka, I.W.; Miyanaga, K.; Hori, K.; Tanji, Y.; Unno, H. Augmentation of self-purification capacity of sewer pipe by immobilizing microbes on the pipe surface. *Biochem. Eng. J.* **2003**, *15*, 69–75. [[CrossRef](#)]
36. Shoji, T.; Matsubara, Y.; Tamaki, S.; Matsuzaka, K.; Satoh, H.; Mino, T. In-sewer treatment system of enhancing self-purification: Performance and oxygen balance in pilot tests. *J. Water Environ. Technol.* **2015**, *13*, 427–439. [[CrossRef](#)]
37. Liang, Z.S.; Zhang, L.; Wu, D.; Chen, G.H.; Jiang, F. Systematic evaluation of a dynamic sewer process model for prediction of odor formation and mitigation in large-scale pressurized sewers in Hong Kong. *Water Res.* **2019**, *154*, 94–103. [[CrossRef](#)] [[PubMed](#)]
38. Æsøy, A.; Storfjell, M.; Mellgren, L.; Helness, H.; Thorvaldsen, G.; Ødegaard, H.; Bentzen, G. A comparison of biofilm growth and water quality changes in sewers with anoxic and anaerobic (septic) conditions. *Water Sci. Technol.* **1997**, *36*, 303–310. [[CrossRef](#)]
39. Pai, T.Y.; Ouyang, C.F.; Liao, Y.C.; Leu, H.G. Oxygen transfer in gravity flow sewer. *Water Sci. Technol.* **2000**, *42*, 417–422. [[CrossRef](#)]